Self-powered Stretchable Sensor Arrays Exhibiting Magnetoelasticity for Real-Time Human-Machine Interaction

Tongtong Zhang, Yi Ding, Chaosheng Hu, Maoyi Zhang, Wenxuan Zhu, Chris R. Bowen, Yu Han, and Ya Yang**

[*] T. Zhang, C. Hu, M. Zhang, W. Zhu, Prof. Y. Yang, CAS Center for Excellence in Nanoscience, Beijing Key Laboratory of Micro-nano Energy and Sensor, Beijing Institute of Nanoenergy and Nanosystems, Chinese Academy of Sciences, Beijing, 101400, P.R. China
E-mail: yayang@binn.cas.cn
Y. Ding and Y. Han, State Key Laboratory of Advanced Power Transmission Technology (State Grid Smart Grid Research Institute Co. Ltd.), Beijing 102209, P.R. China
E-mail: epri313@sina.com.cn
C. R. Bowen, Department of Mechanical Engineering, University of Bath, BA2 7AK, UK
T. Zhang, C. Hu, Prof. Y. Yang, School of Nanoscience and Technology, University of Chinese Academy of Sciences, Beijing, 100049, P. R. China
W. Zhu, Prof. Y. Yang, School of Chemistry and Chemical Engineering, Center on Nanoenergy Research, Guangxi University, Nanning, Guangxi, 530004, P.R. China

Keywords: self-powered, stretchable strain sensors, human-machine interaction, electromagnetic generator, magnetoelasticity.

1. Introduction

With the rapid development of artificial intelligence [1-3] and related applications, stretchable strain sensors [4-6] are able to use mathematical algorithms [7-9] to convert human movement into electrical signals. Such sensors are thereby playing an increasingly important role in next-generation humanoid-robots [10-13], human-machine interaction (HMI) systems [14-16] and human movement monitoring [17-20]. Flexible/stretchable strain sensors are able to withstand a large external strain [18] in contrast to their traditional rigid counterparts. When compared with the traditional keyboards, joysticks and touchpads, stretchable sensors can be

integrated into the surface of a human body, thereby making it a highly attractive approach to measure movement on flexible and curved surfaces. In this regard, with the development of new materials and technologies, the advantages of flexible sensors have gradually emerged and are being widely exploited in HMI systems.

To date, stretchable strain sensors based on the piezoresistive effect [21], capacitance effect [22], surface electromyography [14, 23-25] and triboelectric effect [17, 26-31] have been developed. As an example, M. Boutry *et al.* [32] reported on a capacitor-based biomimetic soft electronic skin that was able to distinguish between normal and tangential forces in real time. K. Suzuki *et al.* [33] designed a carbon nanotube-based resistive strain sensor for real-time monitoring of finger joint motion. However, a number of HMI systems that are based on capacitors and resistive gloves require a battery for sensor operation. In addition, the feedback of complex gestures cannot be readily achieved without powerful signal processing methods, such as machine learning. Emerging energy harvesting technologies[34], such as piezoelectricity and triboelectricity, are able to reduce or remove a reliance on batteries by collecting the mechanical energy associated with human movement, thereby facilitating the development of a self-powered and wearable HMI systems. However, the triboelectric signal can readily be influenced by humidity [35, 36] and temperature [37], and this is particularly important since wearable devices will inevitably be exposed to sweat during operation, which can lead to a decrease in the output of a triboelectric-based strain sensor. In addition, the mechanical stability, material quality, chemical stability or structure of devices contain certain defects [19, 38], resulting in challenges to achieve large-scale production.

The phenomenon of electromagnetic induction was discovered by Faraday [39] in 1831 and is the primary means of electricity generation today. While electromagnetic generators (EMGs) have been employed to produce power, they have rarely been exploited in flexible and wearable devices. To this purpose, we have prepared novel EMG device based on flexible magnets to realize self-powered sensing of flexible wearable devices. The device has the advantage of a

simple structure, is low cost, uses readily available raw materials, and can realize large-scale production.

In this work, we propose a new form of strain sensor based on a flexible NdFeB magnet, which can convert the mechanical energy associated with finger movement into electrical energy to realize a wearable and self-powered sensor. The sensing principle of flexible-NdFeB-magnet-based strain sensor is based on an electromagnetic generator that operates via Faraday's law of electromagnetic induction. The sensor provides a highly linear positive correlation with stretching length, and stretching frequency. The devices can be stretched to a high strain of 400%, as a result of its excellent tensile properties. At a strain level of 60% the output current of the sensing unit after >10,000 stretch-release cycles were quantified. Using a statistical analysis of the measured pulse signal, the degree and direction of finger movement can be determined in real time. As a result, a HMI system is designed to allow remote control of a robot hand and a motor vehicle using a human hand in combination with the sensor, as shown in Figure 1a. This work provides a new scheme for real-time gesture interaction based on electromagnetic generators, to realize intuitive and natural HMI.

2. Results and discussion

2.1. Wearable man-machine interactive system

Fig. 1a shows the main functions and structure of the wearable HMI system, which can remotely detect gestures and operate a robot hand and road vehicle. The wearable HMI system is composed of a soft-magnet-based stretchable sensor array (SMSSA) and a wireless printed circuit board (PCB; see Fig. 1a, b). Due to the structural design of the sensor array and the use of flexible materials, the sensor can be readily attached to the skin of human fingers when subjected to either extended and release states. The PCB that is worn on the hands can integrate a variety of tasks, such as wireless signal transmission, signal processing, and signal conditioning using integrated circuit components, as shown in Fig. 1c. Supplementary Fig. 1 outlines the process flow of the hardware and software, with the initial aquisition of the analog

signal, followed by signal adjustment and processing, and the signal is finally wirelessly transmitted to the robot hand for control and to simulate the movement of a human hand (Fig. 1c). A detailed outline of the workflow is outlined in Supplementary Note 1. The main purpose of the PCB circuit is to amplify the acquired signals, while removing the interference signal and ambient noise through a low-pass filter. As a result of the specificity of different sensors, the signal adjustment pathway of each sensor is achieved by an analog circuit that is associated with the corresponding conversion signal. These factors ensure that the final output of the SMSSA can be accurately received and transmitted to the manipulator or remote-control vehicle via Bluetooth. The approach also lays the foundation for the subsequent processing of the analog-to-digital converter (ADC).

2.2. Structural design and working mechanism

The SMSSA is able to actively convert gesture signals into distinguishable electrical signals and provide an input message into a circuit system. As shown in Fig. 1d, the core of the sensor unit consists of a flexible magnet that is wrapped in a copper coil, which is covered by an Ecoflex sleeve. Compared with traditional permanent magnets, the device can be readily integrated with copper coils and can be subjected to high tensile strains, as seen in Fig. 1e. A scanning electron microscope (SEM) image at different magnifications is shown in Supplementary Fig. 2 to show the sensor microstructure.

All components of the sensing unit are made from economically feasible materials and can be produced through a scaleable manufacturing process; the fabrication method is detailed in Methods and Supplementary Fig. 3. NdFeB powders were selected as the functional material since it can be dispersed in the polymer elastomer matrix. The device can provide electro-mechanical conversion by fixing a conductive coil in the appropriate position, where the coiled conductive structure ensures that the flexible sensing unit maintains a high electrical conductivity under high tensile strain conditions, thus ensuring robustness of the sensing unit. A change in the magnetic flux through the copper coil is achieved during individual stretch-

release cycles, resulting in an induced electromotive force, were Supplementary Fig. 4 illustrates the response principle of the device. In order to visualize the strain and magnetic flux changes during the stretching process, COMSOL was used to simulate the process, where the simulation results are shown in Fig. 2c, d and Supplementary Fig. 5. Faraday's law of electromagnetic induction indicates that an induced current is produced in a closed circuit by a change in the magnetic fluxes that passing through it. The induced current is defined as $I = \frac{N}{R}\frac{\mathrm{d}\varphi}{\mathrm{d}t}$, where N represents the number of copper coils, R is resistance, φ is the magnetic flux, t is time.

2.3. Mechanical and electrical properties characterization

To quantitatively characterize the electrical and mechanical properties of the stretchable sensor unit based on NdFeB/Ecoflex composite film, an actuation motor was used to apply a cyclic tensile load as an input stimulus. Fig. 2a shows the magnitude of the electric current of the sensing unit at a tensile strain of 30% at cycling frequencies of 0.5 Hz to 5Hz. Fig. 2b shows the sensitivity of the sensing unit in the frequency range of 0.5 Hz to 5Hz at the same tensile strain. Fig. 2c shows that the electric current generated by the sensing unit at a cyclic frequency of 5Hz at tensile strains of 20%, 30%, 40%, 50%, 60%, 70% and 80%. According to Supplementary Fig. 6, the current signal changes to a small degree when the strain is greater than 70%, and the level of linearity of the current-strain response reduces. Based on this, Fig. 2d examines current-strain data at a tensile strain range of 20% to 70% at different frequencies for the linear analysis. The strain amplitude and strain frequency of the sensor can be derived by the strain time and current value, where the specific method employed is described in detail in Supplementary Note 3 and Supplementary Fig. 7. The output signal is stable and uniform, and its amplitude is positively correlated with the frequency and tensile strain respectively, which indicates that the sensing unit has the advantages of stable output signal. The sensitivity is defined by $S = \Delta I / \Delta\varepsilon$, where ΔI is the difference in current peak and valley and ε is the strain. According to Figure 2d, an excellent sensitivity from 28.3 μA to 139.4 μA at different frequencies was obtained in a wide strain range of up to 70%. In addition, the line in Fig. 2c

and Fig. 2d is obtained by fitting the sensor current corresponding to each frequency or stretching length, where the output signal is stable at each strain, with a strong R^2 correlation of up to 0.98.

We now discuss the response time of the device during stretch-release cycles in response to external forces, which is a key factor in evaluating the performance of a sensor when undertaking real-time HMI tasks. Here, the *response time* is defined as the time required to transition from its steady-state to a maximum value. Accordingly, the *recovery time* is the time required to recover from the maximum response to the steady-state value. As shown in Fig. 2e, the sensors provide a rapid response to both external loading and unloading, where the device has a response time of approximately 30 ms and a recovery time of approximately 60 ms, enabling the device to sense rapidly changing mechanical stimuli. The output electrical signals are similar to the applied tension, with a negligible time difference under a tension of approximately 1.6 N; see Fig. 2f and Fig. S8.

The durability of the device is also a key characteristic to achieve long-term operation during mechanical cycling. As seen in Fig. 2g, after over 10,000 consecutive stretch-release cycles at a 60% tensile strain, the change in sensor output current is small and less than 2%. The inset in Fig. 2g shows the output current waveforms of the sensor in the initial and final stages of stretch-release cycle process, which remain almost the same. We also explored the effect of different particle sizes and doping ratio on the sensor current signal to determine an appropriate powder size; see Supplementary Fig. 9. In addition, we also evaluated the stress-strain response of the sensor and compared the mechanical properties of sensors of different size and structure, which are shown in Fig. 2h and Supplementary Fig. 10. The device with an inner coil diameter of 3 mm in an Ecoflex matrix exhibited the best mechanical properties, with no significant decrease in stress after 40 cycles of stretching. It can be seen from the inset in Fig. 2h that a 5 cm long sensing unit can be extended four times its original length to 20 cm.

Thus, when compared with the most advanced strain sensors, SMSSAs have a significant advantage of a fast response time, high stretchability, good mechanical durability, and high sensitivity, to provide a rapid and accurate response to gesture instructions via electrical signals. These properties allow the sensor to meet many practical application requirements and are now demonstrated.

2.4. Gesture recognition and its real-time verification in human-machine interaction

The SMSSAs, which are made from flexible materials and designed as stretchable structures, are able to be attached to the surface of a hand or glove to illustrate their potential application (Fig. 1a). To demonstrate the ability of SMSSAs to recognize gestures, we have evaluated the performance of the core functional sensing unit in response to specific finger motions. Supplementary Fig. 11b shows the sensing signals in the form of an electrical current from a sensor unit located on the index finger and correspond to three different motion states. As a result, finger movements can be analyzed using gloves with SMSSAs attached. As the fingers move, information on the motion of each finger is recorded which can be combined into a complex set of electrical signals that correspond to different gestures. The finger data channels are independent of each other and are combined to reflect finger movement, see Fig. 3a. The SMSSAs can accurately identify different numbers such as “8” and “6”, sign language such as “love” and “good” and other corresponding different gestures without interference between the signals; as shown in Fig. 3c (i). Simultaneously, we tested the stability of the system by gesturing the number “6” continuously to produce the signals shown in Fig. 3c (ii) and Movie S2, where the signal values are highly consistent. In Fig. 3c, small peaks appear in the little finger, which is due to the fact that when some fingers are bent, others are often driven unconsciously. Fig. 3c (iii) is the application (APP) screenshot of the system, indicating the gesture of number “6”.

Supplementary Fig. 11 shows that the SMSSA sensor can monitor the degree of bending of fingers in the form of a different peak signal output, which can be used for remote control of

a manipulator. To demonstrate the real-time control capability of the SMSSA-based sensor system, a gloved HMI was integrated with the sensor system to developed a hand controlled manipulator. The SMSSA sensors were installed on the finger to control the bending motion of the robot finger. The manipulator communicates with the sensors via Bluetooth, so that remote control of the robot finger can be achieved, as shown in Fig. 3b. An overview of manipulator's control process is shown in Supplementary Fig. 1, which is connected to the signal processing circuit chip (ADC) that receives data from the sensors and transmits signals to control the manipulator.

As shown in Fig. 3d (i-v), as the human fingers are bent in turn, the fingers of the robot manipulator also bend, where the robot finger motion can achieve almost complete synchronization with the human finger motion. Movie S1 demonstrates the real-time control of the robot hand during bending in sequence. In addition, the SMSSAs also demonstrate high stability during multi-channel control. When specific fingers are bent, other fingers are often unconsciously driven, and the movements can produce false crosstalk signals. The SMSSA-based HMI system can effectively suppress crosstalk between different channels by setting different thresholds, which is important in achieving stable real-time gesture interactions. As shown in Fig. 2c, each electrical signal consists of a crest and a set of troughs, which reflect the bending and stretching of the fingers, respectively. The motion threshold is determined by the mean peak range after several tests. As a result, we can use the SMSSA-based human-machine interaction systems to complete complex gestures, as shown in Fig. 3d (vi-x) and Movie S1.

2.5 Remote control of vehicle in human-machine interaction

To validate the concept of a HMI application, we produced an automatic recognition system which allow humans to use a SMSSA-based HMI system to allow human gestures to interact with a vehicle. The system consists of a data acquisition unit, a wireless data transmission module, a wireless data receiving module and a four-drive vehicle. Each gesture was defined as an individual motion command that related to directional motion, see Fig. 4a.

Firstly, dice was used to randomly determine the required mode of motion of the vehicle, and the accuracy test of each motion command, namely stopping, forward, left and right was completed. The test site layout is shown in Fig. 4c and Movie S3. And since dice rolling has a certain contingency, the number of tests for each movement mode is from 63 to 81. A confusion map of the results is shown in Fig. 4d, where each row of the matrix represents the test sample in an actual category, and each column represents the predicted category. Three of the four gestures achieved a classification accuracy of more than 98%, with the lowest accuracy of 90.1%. In addition, the overall accuracy was 96.8%. Based on this, a maze was designed with "MNES (Micro-Nano Energy Sensors)" as the main geometry.

As shown in Fig. 4e, the maze was a 5 m by 5 m square, and the channel size is slightly wider than the car. While wearing gloves equipped with the SMSSA-based sensors, the test subject stood at the entrance of the maze and monitored the direction of car movement in real time, until the car was out of the maze. Fig. 4f shows photos of the vehicle passing through the maze, which were captured by the vehicle entering - Turn 1- Turn 2 - Turn 3. The whole process is shown in Movie S4. Due to the curves and size constraints of the maze, communication between gestures and vehicle needs to be rapid and accurate, which demonstrates the high accuracy and short response time of the sensor.

Our wearable human-machine interaction system offers several attractive features, and future research directions can include the use of flexible electronics for wireless transmission so that the mechanical flexibility of the sensor system is enhanced. Since the robot structure of can limit sensor functionality, a robot hand that is flexibile in multiple degrees of freedom can be employed to achieve remote analog control of a variety of more complex gestures. Furthermore, research in this area can be devoted to improve the size and structure of the device, further optimize the algorithm framework, and to achieve more functional human-computer interaction.

3. Conclusions

We have developed a wearable human-machine interaction system that exploits a new form of soft-magnet-based stretchable sensor array (SMSSA), which can be used for sign language translation, manipulation, and remote control of vehicles. Compared with other wearable strain sensors, our new NdFeB based sensor has several attractive and innovative features, including high sensitivity, stable operation at high levels of stretch, low cost, uses readily available raw materials, and is self-powered; as outlined in Table S1.

Our SMSSAs are based on electromagnetic generators (EMGs), where the magnetic flux through a copper coil changes during the stretch-release process, which can effectively convert the tensile force or pressure into an electrical signal. The response-recovery time of the SMSSAs is less than 100 ms, while the magnitude of the electrical signal has no observable attenuation change after experiencing over 10,000 consecutive stretch-release cycles, which makes the sensor simple, reliable and efficient to achieve human-machine interaction tasks and the control of robot hands and vehicles. The sensing units of SMSSAs are prepared from economically viable materials that can be scaled up for mass production. The flexible substrate is made of Ecoflex, which has good biocompatibility and can be integrated on the skin surface or woven into the glove. As a result, the electromagnetic generators provide new directions for real-time gesture interaction to realize intuitive and natural human-machine interactions.

4. Experimental Section

Fabrication of the NdFeB-Ecoflex composite materials: $Nd_2Fe_{14}B$ magnetic powders were purchased from Jiangmen Yuhong Co., Ltd. The particle size was 100 mesh (~150 μm). The silicone elastomer (Ecoflex 0020) was purchased from Shanghai Smarttech Co., Ltd. The silicone film was achieved by mixing part A and part B at a ratio of 1:1 in weight. All chemicals did not undergo further treatment.

Fabrication of stretchable strain sensors: The preparation process of the strain sensor is shown in Supplementary Fig. 3. Firstly, a cylinder with a diameter of 3 mm was selected as the mold

for winding copper wires. A flexible conductive copper wire was rolled into a 150-layered spring-like coil with a diameter of approximately 3.0 mm, then it was placed in the center of a cube with a size of 50 mm × 3 mm × 3 mm and engraved by a laser engraving machine, as shown in Supplementary Fig. 3b. Then, Ecoflex A (2 g) and Ecoflex B (2 g) where placed in a beaker and stirred well. A mass of 16 g of $Nd_2Fe_{14}B$ magnetic powders were then blended with the Ecoflex liquid to produce a black and homogeneous mixture; see Supplementary Fig. 3d. The prepared liquid mixture was carefully poured into a hollow cube, and then solidified at 60°C (Supplementary Fig. 3e). The spring section acted as the electrical component while the $Nd_2Fe_{14}B$ magnetic powders were selected as the magnetic part. A 50 mm × 3 mm × 3 mm composite magnetoelectric elastic conductor was manufactured after being magnetized in a high-voltage magnetic field in the axial direction (Supplementary Fig. 3g). The elastic coefficient of the flexible sensor is large, and the stretching process has a significant influence on the performance of the device. Therefore, the prepared sample was placed into a test tube containing Ecoflex colloid and cured at room temperature for one hour to obtain a sensor with a final outer diameter of 5 mm (Supplementary Fig. 3h).

Characterization and measurements: The $Nd_2Fe_{14}B$ magnetic powders and its nanocomposites were characterized using a field-emission scanning electron microscope (SEM, ZEISS GIMINER 300). The specimens were carved by a laser engraving machine (Universal, PLS 4.75). The mechanical tensile tests of the composite materials were conducted on a universal testing machine ESM301-50 N with the tensile mode (100 mm/min). The electrical signals were characterized with a Keithely 2611B system controlled by a computer. The stretching process is provided by a linear motor (LINMOT).

Supporting Information

Supporting Information is available online from the author.

Acknowledgements

This work was supported by the National Natural Science Foundation of China (Grant No. 52072041), the Beijing Natural Science Foundation (Grant No. JQ21007), the Beijing Nova Program (Grant No. Z211100002121086) and the University of Chinese Academy of Sciences (Grant No. Y8540XX2D2).

Received: ((will be filled in by the editorial staff))
Revised: ((will be filled in by the editorial staff))
Published online: ((will be filled in by the editorial staff))

References

[1] C. Kaspar, B. J. Ravoo, W. G. van der Wiel, S. V. Wegner, W. H. P. Pernice, *Nature* **2021**, 594, 345-355.

[2] N. D. Lane, S. Bhattacharya, A. Mathur, P. Georgiev, C. Forlivesi, F. Kawsar, *Ieee Pervas. Comput.* **2017**, 16, 82-88.

[3] S. Xu, A. Jayaraman, J. A. Rogers, *Nature* **2019**, 571, 319-321.

[4] M. Amjadi, K. U. Kyung, I. Park, M. Sitti, *Adv. Funct. Mater.* **2016**, 26, 1678-1698.

[5] H. T. Yang, J. L. Li, K. Z. Lim, C. J. Pan, T. V. Truong, Q. Wang, K. R. Li, S. Li, X. Xiao, M. Ding, T. L. Chen, X. L. Liu, Q. Xie, P. V. Y. Alvarado, X. N. Wang, P. Y. Chen, *Nat. Mach. Intell.* **2022**, 4, 84-94.

[6] J. Lee, S. J. Ihle, G. S. Pellegrino, H. Kim, J. Yea, C. Y. Jeon, H. C. Son, C. Jin, D. Eberli, F. Schmid, B. L. Zambrano, A. F. Renz, C. Forro, H. Choi, K. I. Jang, R. Kung, J. Voros, *Nat. Electron.* **2021**, 4, 291-301.

[7] M. Wang, Z. Yan, T. Wang, P. Q. Cai, S. Y. Gao, Y. Zeng, C. J. Wan, H. Wang, L. Pan, J. C. Yu, S. W. Pan, K. He, J. Lu, X. D. Chen, *Nat. Electron.* **2020**, 3, 563-570.

[8] Z. H. Zhou, K. Chen, X. S. Li, S. L. Zhang, Y. F. Wu, Y. H. Zhou, K. Y. Meng, C. C. Sun, Q. He, W. J. Fan, E. D. Fan, Z. W. Lin, X. L. Tan, W. L. Deng, J. Yang, J. Chen, *Nat. Electron.* **2020**, 3, 571-578.

[9] Y. Y. Luo, Y. Z. Li, P. Sharma, W. Shou, K. Wu, M. Foshey, B. C. Li, T. Palacios, A. Torralba, W. Matusik, *Nat. Electron.* **2021**, 4, 193-201.

[10] T. Belpaeme, J. Kennedy, A. Ramachandran, B. Scassellati, F. Tanaka, *Sci. Robot.* **2018**, 3, eaat5954.

[11] A. S. Niyetkaliyev, S. Hussain, M. H. Ghayesh, G. Alici, *Ieee T. Hum-Mach. Syst.* **2017**, 47, 1134-1145.

[12] C. Laschi, B. Mazzolai, M. Cianchetti, *Sci. Robot.* **2016**, 1, eaat5954.

[13] P. Polygerinos, N. Correll, S. A. Morin, B. Mosadegh, C. D. Onal, K. Petersen, M. Cianchetti, M. T. Tolley, R. F. Shepherd, *Adv. Eng. Mater.* **2017**, 19, 1700016.

[14] S. S. Rautaray, A. Agrawal, *Artif. Intell. Rev.* **2015**, 43, 1-54.

[15] S. Lim, D. Son, J. Kim, Y. B. Lee, J. K. Song, S. Choi, D. J. Lee, J. H. Kim, M. Lee, T. Hyeon, D. H. Kim, *Adv. Funct. Mater.* **2015**, 25, 375-383.

[16] P. K. Pisharady, P. Vadakkepat, A. P. Loh, *Int. J. Comput. Vision.* **2013**, 101, 403-419.

[17] C. Y. Li, D. Liu, C. Q. Xu, Z. M. Wang, S. Shu, Z. R. Sun, W. Tang, Z. L. Wang, *Nat. Commun.* **2021**, 12, 2950.

[18] C. Q. Dong, A. Leber, T. Das Gupta, R. Chandran, M. Volpi, Y. P. Qu, N. D. Tung, N. Bartolomei, W. Yan, F. Sorin, *Nat. Commun.* **2020**, 11, 3537.

[19] C. X. Tan, Z. G. Dong, Y. H. Li, H. G. Zhao, X. Y. Huang, Z. C. Zhou, J. W. Jiang, Y. Z. Long, P. K. Jiang, T. Y. Zhang, B. Sun, *Nat. Commun.* **2020**, 11, 3530.

[20] D. Zhang, K. W. Zhang, Y. M. Wang, Y. H. Wang, Y. Yang, *Nano Energy* **2019**, 56, 25-32.

[21] J. M. Gu, J. Ahn, J. Y. Jung, S. Cho, J. Choi, Y. Jeong, J. Park, S. Hwang, I. Cho, J. Ko, J. H. Ha, Z. J. Zhao, S. Jeon, S. Ryu, J. H. Jeong, I. Park, *Nano Energy* **2021**, 89, 106447.

[22] K. Y. Chun, Y. Oh, J. Rho, J. H. Ahn, Y. J. Kim, H. R. Choi, S. Baik, *Nat. Nanotechnol.* **2010**, 5, 853-857.

[23] A. Moin, A. Zhou, A. Rahimi, A. Menon, S. Benatti, G. Alexandrov, S. Tamakloe, J. N. Ting, N. Yamamoto, Y. Khan, F. Burghardt, L. Benini, A. C. Arias, J. M. Rabaey, *Nat. Electron.* **2021**, 4, 54-63.

[24] L. X. Tang, J. Shang, X. Y. Jiang, *Sci. Adv.* **2021**, 7, eabe3778.

[25] D. Tkach, H. Huang, T. A. Kuiken, *J. Neuroeng. Rehabil.* **2010**, 7, 21.

[26] T. Jin, Z. D. Sun, L. Li, Q. Zhang, M. L. Zhu, Z. X. Zhang, G. J. Yuan, T. Chen, Y. Z. Tian, X. Y. Hou, C. Lee, *Nat. Commun.* **2020**, 11, 5381.

[27] F. Wen, Z. D. Sun, T. Y. Y. He, Q. F. Shi, M. L. Zhu, Z. X. Zhang, L. H. Li, T. Zhang, C. K. Lee, *Adv. Sci.* **2020**, 7, 2000261.

[28] K. Qin, C. Chen, X. J. Pu, Q. Tang, W. C. He, Y. K. Liu, Q. X. Zeng, G. L. Liu, H. Y. Guo, C. G. Hu, *Nano-Micro Lett.* **2021**, 13, 51.

[29] Y. Wang, H. Wu, L. Xu, H. Zhang, Y. Yang, Z. L. Wang, *Sci Adv* **2020**, 6, eabb9083.

[30] C. Zhao, D. H. Liu, Y. W. Wang, Z. Y. Hu, Q. Q. Zhang, Z. Y. Zhang, H. Wang, T. L. Du, Y. J. Zou, H. C. Yuan, X. X. Pan, J. C. Mi, M. Y. Xu, *Nano Energy* **2022**, 94, 106926.

[31] J. Chen, Z. L. Wang, *Joule* **2017**, 1, 480-521.

[32] C. M. Boutry, M. Negre, M. Jorda, O. Vardoulis, A. Chortos, O. Khatib, Z. N. Bao, *Sci. Robot.* **2018**, 3, eaau6914.

[33] K. Suzuki, K. Yataka, Y. Okumiya, S. Sakakibara, K. Sako, H. Mimura, Y. Inoue, *Acs Sensors* **2016**, 1, 817-825.

[34] Q. G. Li, V. Naing, J. M. Donelan, *J. Neuroeng. Rehabil.* **2009**, 6, 22.

[35] W. F. Yang, W. Gong, C. Y. Hou, Y. Su, Y. B. Guo, W. Zhang, Y. G. Li, Q. H. Zhang, H. Z. Wang, *Nat. Commun.* **2019**, 10, 5541.

[36] Y. Q. Hu, X. L. Wang, H. K. Li, H. Q. Li, Z. H. Li, *Nano Energy* **2020**, 71, 104640.

[37] C. X. Lu, C. B. Han, G. Q. Gu, J. Chen, Z. W. Yang, T. Jiang, C. He, Z. L. Wang, *Adv. Eng. Mater.* **2017**, 19*,* 1700275.

[38] C. M. Boutry, Y. Kaizawa, B. C. Schroeder, A. Chortos, A. Legrand, Z. Wang, J. Chang, P. Fox, Z. N. Bao, *Nat. Electron.* **2018**, 1, 314-321.

[39] J. Al-Khalili, Philos Trans A Math Phys Eng Sci 2015, 373.

[40] J. D. Shi, S. Y. Lv, L. Wang, Z. H. Dai, S. T. Yang, L. Y. Zhao, H. H. Tian, M. D. Du, H. B. Li, Y. Fang, *Adv. Mater. Interfaces.* **2019**, 6, 1901223.

[41] J. Zhou, X. Z. Xu, Y. Y. Xin, G. Lubineau, *Adv. Funct. Mater.* **2018**, 28, 1705591.

FIGURE CAPTIONS

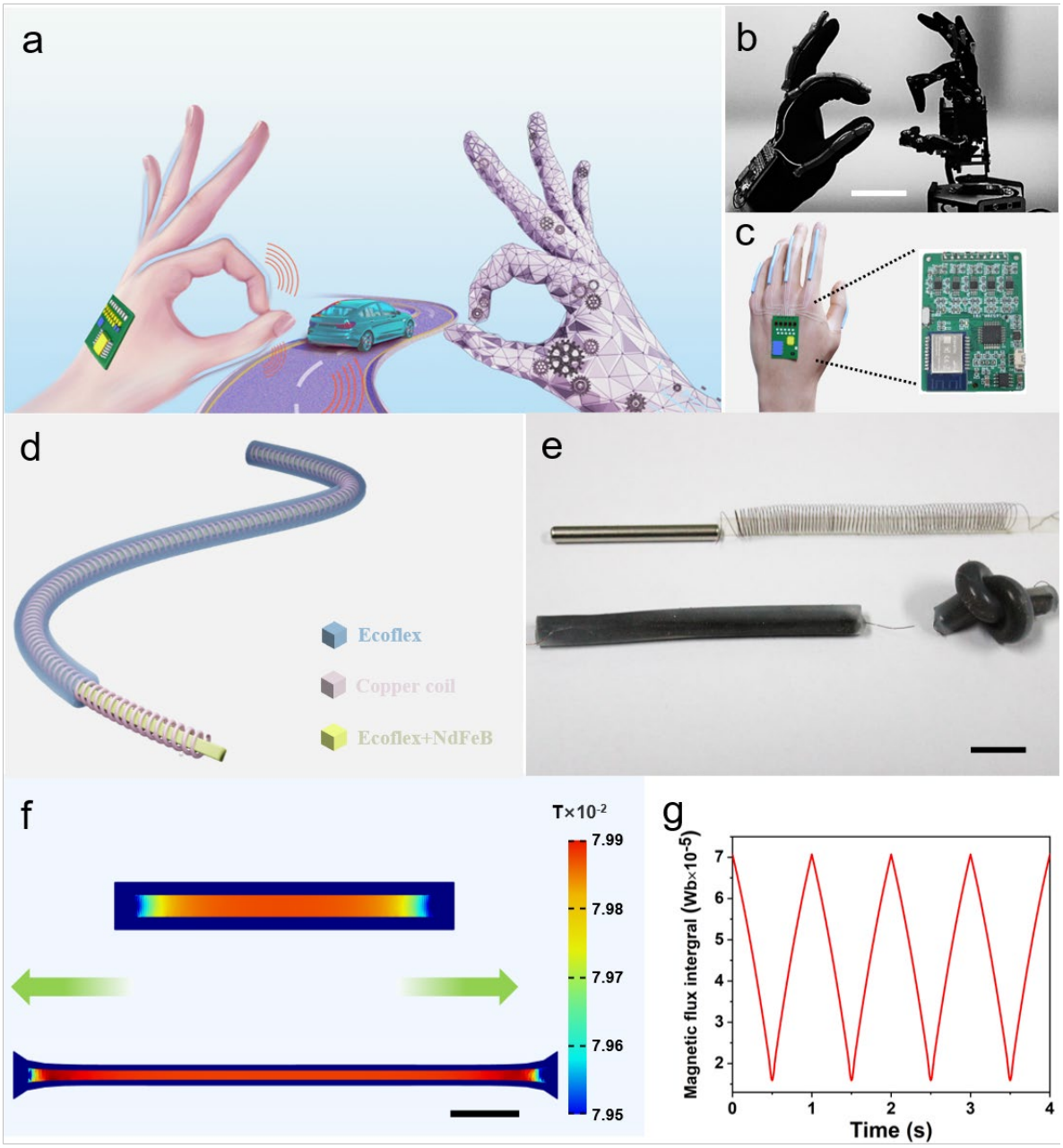

Figure 1. Schematic of the wearable HMI system and its working mechanism. a) Schematic of the HMI system. b) Schematic of a hand wearing a number of SMSSAs along the fingers and a wireless PCB. Scale bar in b, 3 cm. c) Photograph of a hand and the manipulator, with the same gesture. d) Schematic of the soft-magnet-based flexible sensor unit. e) Picture displaying main parts and the sensor after assembly. Scale bar in e, 10 mm. f) and g) Simulation results of the tensile deformation of the sensing unit. Scale bar in c, 10 mm.

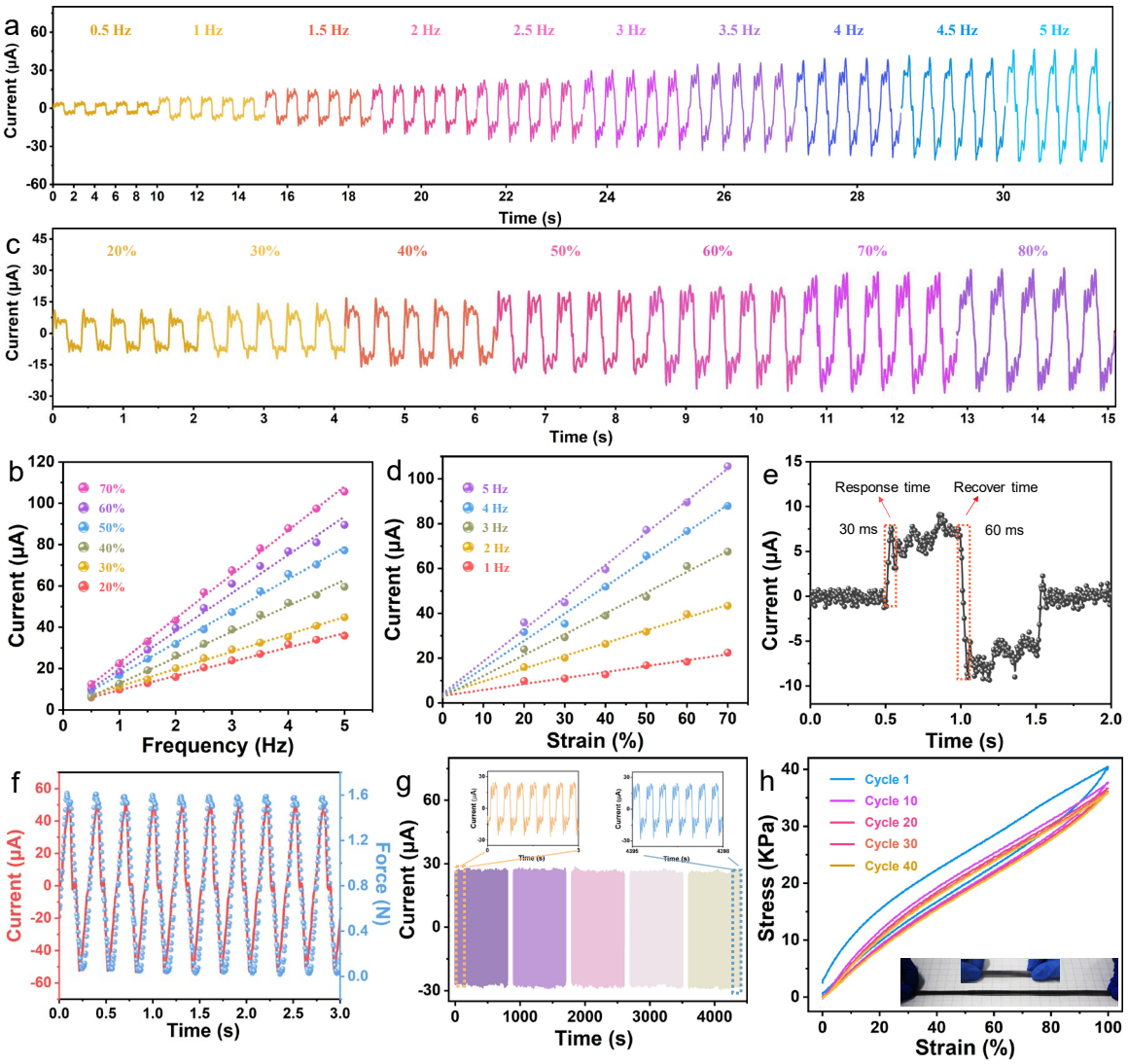

Figure. 2. Electrical characteristics of the sensor response to tension. a) Sensor current monotonically increases with stretching frequency change from 0.5 Hz - 5 Hz. b) Measured output current as a function of stretching frequency. c) Sensor current monotonically increases with change in elongation length from 20% - 100% strain. d) Measured output current as a function of strain. e) *I-T* curve displaying fast response time of 30 ms and recovery time of 60 ms. f) Waveforms of output current and external tension are maintained in step with loading and unloading. g) Mechanical durability test for up to 10,000 continuous stretch–release cycles at 60% strain, showing high stability and repeatability. Inset: the enlarged view of the marked region. h) Cyclical stress-strain curves of the device for 40 times. Inset: photograph of the 5-cm-long sensing unit that can be stretched to 20 cm.

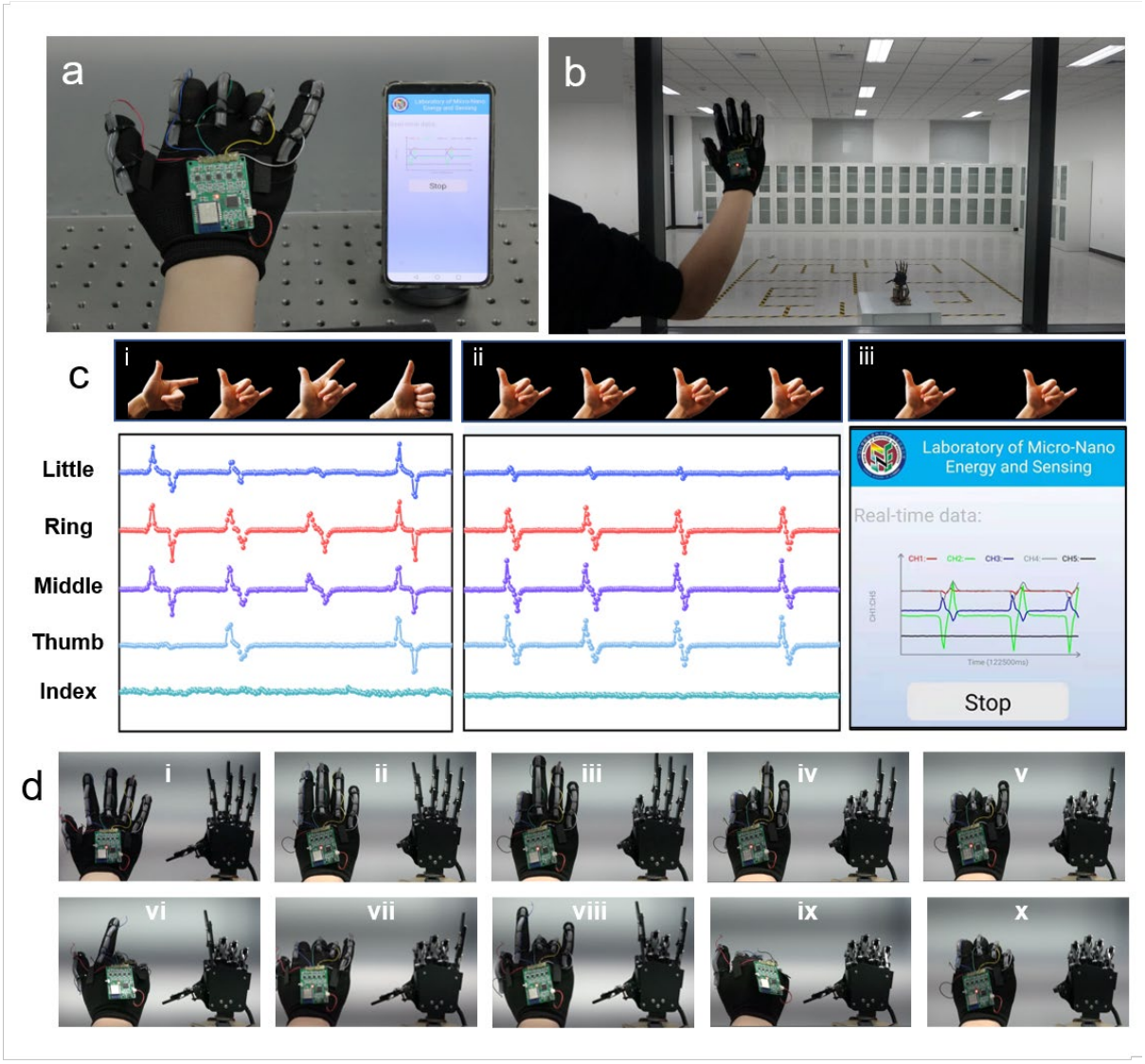

Figure. 3. Real-time interactive gesture demonstration. a) Photograph of SMSSA-based gesture translation system. b) photograph of the robot hand movement controlled by the SMSSA-based human-machine interaction systems in real time. c) (i) Electrical signals of different gestures. (ii) Stability of the SMSSA-based gesture translation system. (iii) APP screenshot of the system. d) SMSSA-based human-machine interaction systems that controls the movement of the robot hand.

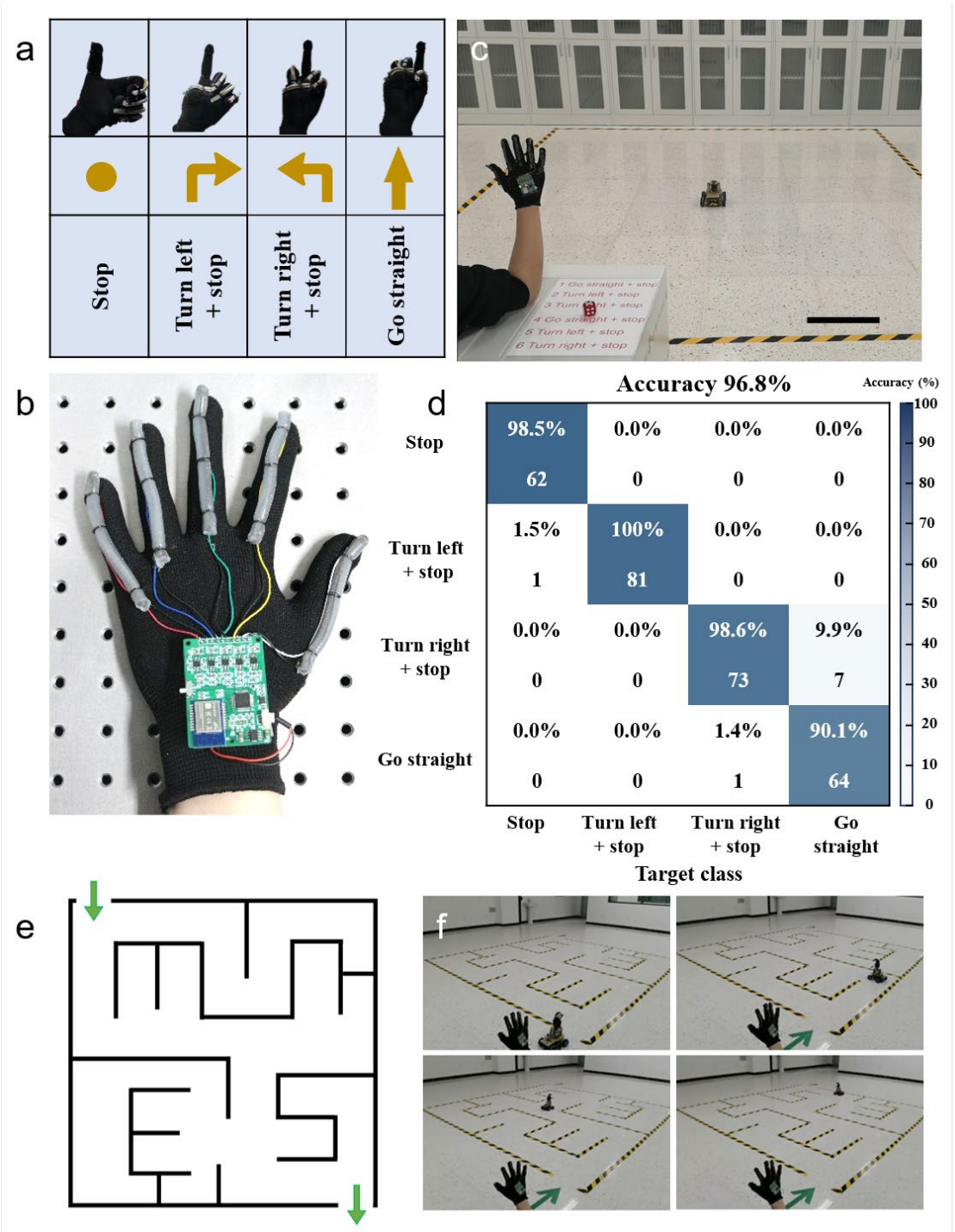

Figure. 4. Real-time interactive gesture demonstration. a) Each of the four categories of hand gestures was appointed a specific motor command to guide the movement of the vehicle. b) Photograph showing the installation of the SMSSAs on a glove. c) Photograph of accuracy site layout. Scale bar in c, 0.5 m. d) Classification test confusion matrix of 289 test data sets; each row and each column represent an instance of the predicted class and the actual class, and the diagonal value represents the correct result. The color bars indicate the number of predicted numbers. e) Scenarios of the vehicle walking through the labyrinth based on the HMI system. f) Photograph of the vehicle passing through the maze.

TOC

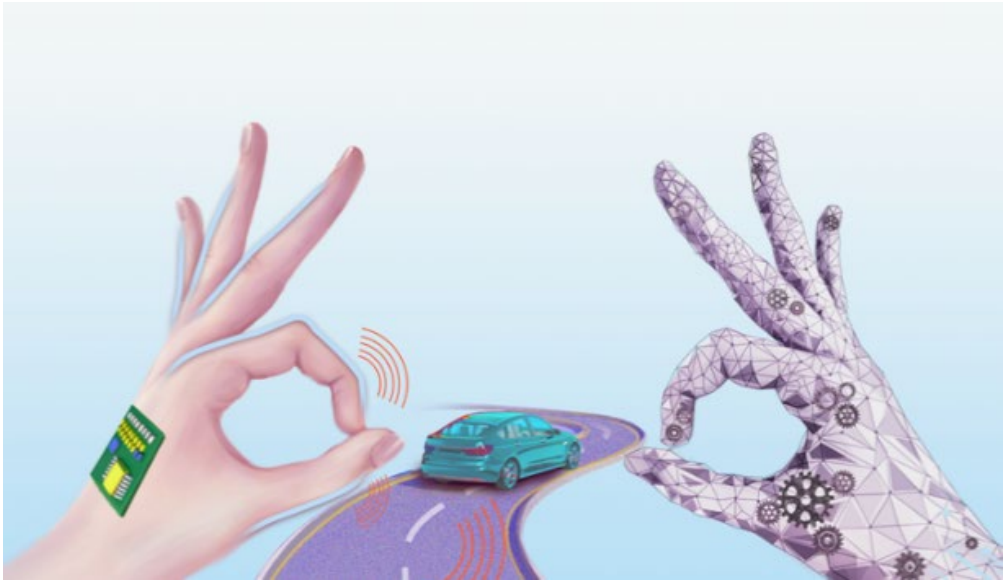

Title: Self-powered Stretchable Sensor Arrays Exhibiting Magnetoelasticity for Real-Time Human-Machine Interaction

TOC text: This work reports a strain sensor based on a flexible NdFeB magnet to realize a wearable and self-powered sensor, which provides open prospects for real-time gesture interaction based on an electromagnetic generator, and is expected to achieve a wide range of future applications for intuitive and natural human-machine interfaces.

Keywords: self-powered, stretchable strain sensors, human-machine interaction, electromagnetic generator, magnetoelasticity.

Authors: Tongtong Zhang, Yi Ding, Chaosheng Hu, Maoyi Zhang, Wenxuan Zhu, Chris R. Bowen, Yu Han*, and Ya Yang*

Abstract: Stretchable strain sensors are highly desirable for human motion monitoring, and can be used to build new forms of bionic robot. However, the current use of flexible strain gauges is hindered by the need for an external power supply, and the demand for long-term operation. Here, we present a new flexible self-powered strain sensor system based on an electromagnetic generator which possesses a high stretchability in excess of 150%, a short response time of 30 ms, and an excellent linearity ($R^2 > 0.98$). Based on this new form of sensor, a human-machine interaction (HMI) system was designed to achieve remote control of a robot hand and vehicle using a human hand, which provides a new scheme for real-time gesture interaction.